Conjugated Oligomers and Polymers of *cis*- and *trans*-Platinum(II)-*para*- and *ortho*-bis(ethynylbenzene)quinone Diimine

Karl Gagnon,[†] Shawkat Mohammed Aly,[†] Anne Brisach-Wittmeyer,[†] Diana Bellows,[†] Jean-François Bérubé,[†] Laurence Caron,[†] Alaa S. Abd-El-Aziz,[‡] Daniel Fortin,*[,†] and Pierre D. Harvey*[,†]

Département de Chimie, Université de Sherbrooke, Sherbrooke, PQ, Canada J1K 2R1, and Department of Chemistry, University of British Columbia, Okanagan, 3333 University Way, Kelowna, BC, Canada V1V 1V7

Received October 20, 2007

Three conjugated polymers of the type $(-\text{spacer}-C\equiv C-PtL_2-C\equiv C-)_n$, with spacer = *para*- and *ortho*-bis(diphenyl(tetramethoxy)quinone diimine) and L = PEt_3, were synthesized as the *cis*- and *trans*-isomers about the Pt. The three combinations (spacer/PtL_2Cl_2), *ortho/trans*, *para/trans*, and *para/cis* led to polydispersed polymers, which upon fractionation provided more monodispersed materials with M_n ranging from 3600 to 32400 (GPC). The spacer *ortho*-bis(diphenylethynyl)tetramethoxyquinone diimine reacts with *cis*-PtL_2Cl_2 to form small oligomers and a chelate cyclic complex (**7**), which was used as a model compound. All materials along with the aryl$-C\equiv C-PtL_2-C\equiv C-$aryl models (L = PEt_3; aryl = C_6H_5, 2,4,6-$C_6H_2Me_3$; 2,4,5-$C_6H_2Me_3$) were studied by ^1H and ^{31}P NMR, IR, UV–vis, TGA, DSC, luminescence spectroscopy, photophysics, and cyclic voltammetry. The UV–vis spectra exhibit an intramolecular low-energy and low-intensity charge transfer band (CT) assigned to $\pi(Ph-C\equiv C)$ (for organics) and $\pi/d_{xy}((Ph-C\equiv C)_2Pt)$ (for organometallics) to the π^*(quinone diimine), as demonstrated by comparison with a corresponding amine derivative (i.e., no CT band) and corroborated by DFT and TDDFT. The polymers and **7** are not luminescent at room temperature (solid and solution). However in 2MeTHF at 77 K, the polymers bearing the combination *ortho/trans* and *para/cis* as well as the model compound **7** exhibit higher energy phosphorescence ($T_n \rightarrow S_0$) originating from the $\pi\pi^*/d_{xy}((Ph-C\equiv C)_2Pt)$ excited states. A correlation between the structural parameters (angle made by the $PtP_2(C\equiv C)_2$ vs the aryl planes, angle made by the aryl and the quinone diimine planes, molecular weight) with the calculated oscillator strength, absorptivities, and the observed position of the lowest energy absorption bands is demonstrated. Finally, upper energy delayed fluorescence ($S_n \rightarrow S_0$) was detected for the polymers and **7** at 77 K and was assigned to T_1-T_1 interactions via aggregation as its intensity varies with the concentration.

Introduction

The use of metal-containing macromolecules have been the topics of intense research for the past 10 years or so, and important applications such as semi- and photoconducting and optical materials, catalysis, and nanomaterials were reported. Reviews on the topics have indeed flourished at a fast rate during the past 5 years or so.[1,2] Among the building blocks for the preparation of these novel materials, one finds the well-known metal-containing fragment bis(ethynylaryl)bis(phosphine)platinum(II), $Ar-C\equiv C-PtL_2-C\equiv C-Ar$ (Chart 1; L = monophosphine), which can be used to prepare innovative conjugated coordination and organometallic cyclic and acyclic oligomers, polymers, dendrimers, and star-shaped molecules.[3] At the same time, both the *trans*- and *cis*-$Ar-C\equiv C-PtL_2-C\equiv C-Ar$ units and alike turn out to be photo- and electroluminescent chromophores,[4] and their excited-state characteristics have attracted some attention from a theoretical point of view.[5]

Chart 1[a]

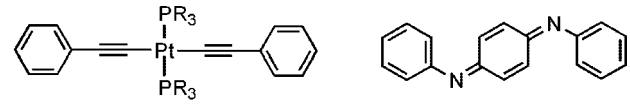

trans-bis(ethynylbenzene)bis(phosphine)platinum(II) *trans*-quinone diphenyldiimine

[a] R = alkyl group.

In parallel, quinone diimine is a nonluminescent chromophore but exhibits electroresponsive properties in acidic solution.[6]

* To whom correspondence should be addressed. Tel: 819-821-7092. Fax: 819-821-8017. E-mail: Pierre.Harvey@USherbrooke.ca.

[†] Université de Sherbrooke.

[‡] UBC Okanagan.

(1) (a) Wong, W.-Y. *Coord. Chem. Rev.* **2007**, *251*, 2400–2427. (b) Herbert, D. E.; Mayer, U. F. J.; Manners, I. *Angew. Chem., Int. Ed.* **2007**, *46*, 5060–5081. (c) Williams, K. A.; Boydston, A. J.; Bielawski, C. W. *Chem. Soc. Rev.* **2007**, *36*, 729–744. (d) Leung, A. C. W.; MacLachlan, M. J. *J. Inorg. Organomet. Polym. Mat.* **2007**, *17*, 57–89. (e) Jiang, J.; Yang, W.; Cao, Y. *J. Inorg. Organomet. Polym. Mater.* **2007**, *17*, 37–55. (f) Marin, V.; Holder, E.; Hoogenboom, R.; Schubert, U. S. *Chem. Soc. Rev.* **2007**, *36*, 618–635. (g) Cheetham, A. K.; Rao, C. N. R.; Feller, R. K. *Chem. Commun.* **2006**, 4780–4795. (h) Wolf, M. *O J. Inorg. Organomet. Polym. Mater.* **2006**, *16*, 189–199. (i) Wong, W.-Y.; Ho, C.-L. *Coord. Chem. Rev.* **2006**, *250*, 2627–2690. (j) Weder, C. *J. Inorg. Organomet. Polym. Mater.* **2006**, *16*, 101–113. (k) Puddephatt, R. J. *J. Inorg. Organomet. Polym. Mater.* **2006**, *15*, 371–388. (l) Chan, W. K. *Coord. Chem. Rev.* **2007**, *251*, 2104–2118.

(2) (a) Harvey, P. D. In *Macromolecule Containing Metal and Metal-like Elements*, Vol. 5; Abd-El-Aziz, A. S., Carraher, C. E., Jr., Zeldin, M., Eds.; Wiley Interscience: New York, 2005; Chapters 4, pp 83–116. (b) Harvey, P. D. In *Frontiers in Transition Metal-Containing Polymers*; Abd-El-Aziz, A. S., Manners, I., Eds.; Wiley Interscience: New York, 2007; pp 321–368. (c) Harvey, P. D. *J. Inorg. Organomet. Polym.* **2004**, *14*, 211–226. (d) Harvey, P. D. *Macromol. Symp.* **2003**, *196*, 173–185. (e) Harvey, P. D. *Coord. Chem. Rev.* **2001**, *219* (221), 17–52. (f) Harvey, P. D. *Macromol. Symp.* **2004**, *209*, 67–79. (g) Harvey, P. D. *Macromol. Symp.* **2004**, *209*, 81–95. (h) Harvey, P. D. *Coord. Chem. Rev.* **2001**, *219* (221), 17–52.

10.1021/om7010563 CCC: $40.75
Publication on Web 04/18/2008

Along with its reduced form, *N*,*N*′-diphenyl-1,4-phenylenediamine, quinone diimine was often investigated in relation with the well-known conducting polymer polyaniline in its protonated emaraldine form.[7]

We now wish to report new conjugated organometallic polymers exhibiting the general structure (−[ethynylbenzene−metal−ethynylbenzene]−[quinone diimine]−)$_n$ where the [ethynylbenzene−metal−ethynylbenzene] is the *trans*- or *cis*-$PtL_2(C{\equiv}CC_6H_4{-})_2$ unit and the [quinone diimine] moiety is the *para*- or *ortho*-substituted bis(ethynylbenzene)-*N*,*N*′-tetramethoxyquinone diimine (Chart 2). The photophysical properties for the *ortho/trans*- and *para/cis*-polymers and the mononuclear complex made of the *ortho/cis* combination turned out to exhibit luminescence arising from upper excited states at 77 K. The *para/trans*-polymer turns out not to be luminescent.

Chart 2

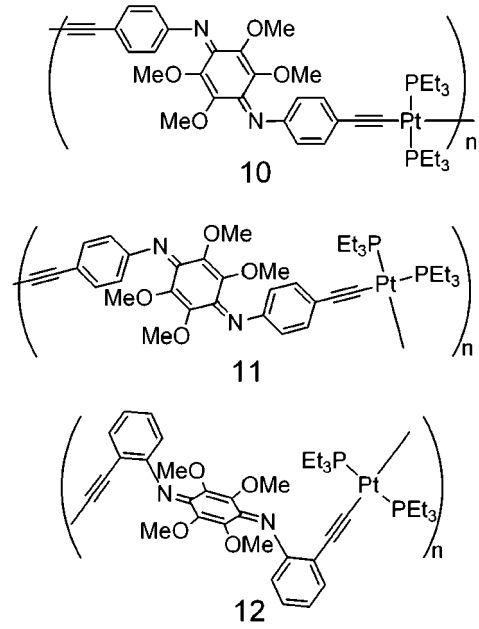

Chart 3

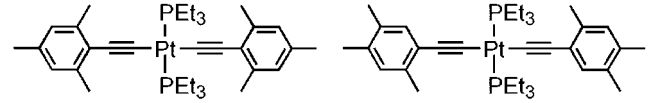

1 **2**

Results and Discussion

Synthesis of the Model Compounds. The model compounds **1** and **2** (Chart 3) were prepared by reacting respectively 2,4,6- and 2,4,5-trimethylphenylacetylene with the *trans*-$Pt(PEt_3)_2Cl_2$ complex in the presence of $^{i}Pr_2NH$. These derivatives were selected in order to provide specific structural information about the *trans*-$PtL_2(C{\equiv}C)_2$ segment and for assignment purposes in the polymers (*cis* vs *trans* about Pt using ^{31}P NMR). Similarly, a study of the electrochemical, optical, and photophysical properties of these models helps understand the photonic properties of the polymers.

The X-ray structures for **1** and **2** (Figure 1) reveal the anticipated *trans*-geometry in both complexes, which turn out to be crystallographically centrosymmetric at the Pt atom. Two different orientations of the aryls with respect to the $PtP_2(C{\equiv}C)_2$ plane are noted, demonstrating at first glance no obvious preference for the parallel or perpendicular orientations of the aryl π-orbitals vs this Pt-containing plane. In **1**, the aryl groups are placed near perpendicular to the $PtP_2(C{\equiv}C)_2$ plane (83.0°). This orientation may be induced by steric effects generated by the two *ortho* methyl groups of the mesityl residues and the PEt_3 ligands. Noteworthy, this compound appears white as crystals. In **2**, there are fewer steric effects (just one *ortho* methyl instead of two). The aryls are oriented more parallel with the $PtP_2(C{\equiv}C)_2$ plane (29.8°), which allows a different alignment of the aryl π-system with respect to the d Pt orbitals. Interestingly, the compound exhibits a yellowish coloration. Again, steric hindrance between the methyl groups and the PEt_3 ligand

(3) (a) Onisuka, K.; Yabe, K.-I.; Ohshiro, N.; Shimizu, A.; Okumura, R.; Takei, F.; Takahashi, S. *Macromolecules* **2004**, *37*, 8204–8211. (b) Lee, S. J.; Hu, A.; Lin, W. *J. Am. Chem. Soc.* **2002**, *124*, 12948–12949. (c) Onitsuka, K.; Shimizu, A.; Takahashi, S. *Chem. Commun.* **2003**, 280–281. (d) Campbell, K.; Johnson, C. A.; McDonald, R.; Ferguson, M. J.; Haley, M. M.; Tykwinski, R. R. *Angew. Chem., Int. Ed.* **2004**, *43*, 5967–5971. (e) Ohshiro, N.; Takei, F.; Onitsuka, K.; Takahashi, S. *J. Organomet. Chem.* **1998**, *569*, 195–202. (f) Huang, C.-C.; Lin, Y.-C.; Lin, P.-Y.; Chen, Y.-J. *Eur. J. Org. Chem.* **2006**, 4510–4518. (g) Onitsuka, K.; Fujimoto, M.; Ohsiro, N.; Takahashi, S. *Angew. Chem., Int. Ed.* **1999**, *38*, 689–692. (h) Onitsuka, K.; Fujumoto, M.; Kitajima, H.; Ohshiro, N.; Takei, F.; Takahashi, S. *Chem.−Eur. J.* **2004**, *10*, 6433–6446. (i) Köhler, A.; Wilson, J. S.; Friend, R. H.; Gerhard, A.; Bässler, H. *J. Chem. Phys.* **2002**, *116*, 9457–9463. (j) Köhler, A.; Beljonne, D. *Adv. Funct. Mater.* **2004**, *14*, 11–18. (k) Ohshiro, N.; Shimizu, A.; Okumura, R.; Takei, F.; Onitsuka, K. J.; Takahashi, S. *Chem. Lett.* **2000**, 786–787. (l) Vicente, J.; Chicote, M.-T.; Alvarez-Falcon, M. M. *Organometallics* **2005**, *24*, 2764–2772. (m) Khan, M. S.; A-Mandhary, M. R. A.; Al-Suti, M. K.; Al-Battashi, F. R.; Al-Saadi, S.; Ahrens, B.; Bjernemose, J. K.; Mahon, M. F.; Raithby, P. R.; Younus, M.; Chawdhury, N.; Köhler, A.; Marseglia, E. A.; Tedesco, E.; Feeder, N.; Teat, S. J. *Dalton* **2004**, *237*, 7–2385. (n) La Groia, A.; Ricci, A.; Bassetti, M.; Masi, D.; Bianchini, C.; Lo Sterzo, C. *J. Organomet. Chem.* **2003**, *683*, 406–420. (o) Köhler, A.; Wittmann, H. F.; Friend, R. H.; Khan, M. S.; Lewis, J. *Synth. Met.* **1994**, *67*, 245–249. (p) Jiang, H.; Lin, W. J. *Organomet. Chem.* **2005**, *690*, 5159–5169. (q) Whittel, G. R.; Manners, I. *Adv. Mater.* **2007**, *19*, 3439–3468.

(4) (a) Lindgren, M.; Minaev, B.; Glimsdal, E.; Vestberg, R.; Westlund, R.; Malmström, E. *J. Lumin.* **2007**, *124*, 302–310. (b) Glimsdal, E.; Carlsson, M.; Eliasson, B.; Minaev, B.; Lindgren, J. *Phys. Chem. A* **2007**, *111*, 244–250. (c) El Hamaoui, B.; Laquai, F.; Baluschev, S.; Wu, J.; Muellen, K. *Synth. Met.* **2006**, *156*, 1182–1186. (d) Kim, K.-Y.; Liu, S.; Koese, M. E.; Schanze, K. S. *Inorg. Chem.* **2006**, *45*, 2509–2519. (e) Danilov, E. O.; Pomestchenko, I. E.; Kinayyigit, S.; Gentili, P. L.; Hissler, M.; Ziessel, R.; Castellano, F. N. *J. Phys. Chem. A* **2005**, *109*, 2465–2471. (f) Tao, C.-H.; Zhu, N.; Yam, V. W.-W. *Chem.−Eur. J.* **2005**, *11*, 1647–1657. (g) Saha, R.; Qaium, Md. A.; Debnath, D.; Younus, M.; Chawdhury, N.; Sultana, N.; Kociok-Koehn, G.; Ooi, L.-L.; Raithby, P. R.; Kijima, M. *J. Chem. Soc., Dalton Trans.* **2005**, *276*, 0–2765. (h) Song, J.-E.; Kim, B.-O.; Ha, Y. *Mater. Sci. Eng. C* **2004**, *24*, 191–194. (i) Pomestchenko, I. E.; Castellano, F. N. *J. Phys. Chem. A* **2004**, *108*, 3485–3492. (j) Rogers, J. E.; Hall, B. C.; Hufnagle, D. C.; Slagle, J. E.; Ault, A. P.; McLean, D. G.; Fleitz, P. A.; Cooper, T. M. *J. Chem. Phys.* **2005**, *122*, 214708. (k) Emmert, L. A.; Choi, W.; Marshall, J. A.; Yang, J.; Meyer, L. A.; Brozik, J. A. *J. Phys. Chem. A* **2003**, *107*, 11340–11346. (l) Liu, Y.; Jiang, S.; Glusac, K.; Powell, D. H.; Anderson, D. F.; Schanze, K. S. *J. Am. Chem. Soc.* **2002**, *124*, 12412–12413. (m) Benito, J.; Berenguer, J. R.; Fornies, J.; Gil, B.; Gomez, J.; Lalinde, E. *J. Chem. Soc., Dalton. Trans.* **2003**, 4331–4339. (n) Rogers, J. J.; Cooper, T. M.; Fleitz, P. A.; Glass, D. J.; McLean, D. G. *J. Phys. Chem. A* **2002**, *106*, 10108–10115. (o) Cooper, T. M.; McLean, D. G.; Rogers, J. E. *Chem. Phys. Lett.* **2001**, *349*, 31–36. (p) Hissler, M,; Harriman, A.; Khatyr, A.; Ziessel, R *Chem.−Eur. J.* **1999**, *336*, 6–3381.

(5) Batista, E. R.; Martin, R. L. *J. Phys. Chem. A* **2005**, *109*, 9856–9859.

(6) (a) de Santana, H.; Quillard, S.; Fayad, E.; Louarn, G. *Synth. Met.* **2006**, *156*, 81–85. (b) Han, C.-C.; Balakumar, R.; Thirumalai, D.; Chung, M.-T. *Org. Biomol. Chem.* **2006**, *4*, 3511–3516. (c) Nishiumi, T.; Chimoto, Y.; Hagiwara, Y.; Higuchi, M.; Yamamoto, K. *Macromolecules* **2004**, *37*, 2661–2664. (d) Nishiumi, T.; Nomura, Y.; Chimoto, Y.; Higuchi, M.; Yamamoto, K. *J. Phys. Chem. B* **2004**, *108*, 7992–8000. (e) Temme, O.; Laschat, S.; Frohlich, R.; Wibbeling, B.; Heinze, J.; Hauser, P. *J. Chem. Soc., Perkin Trans. 2* **1997**, 2083–2085.

(7) (a) Ding, Y.; Boone, H. W.; Anderson, J. D.; Padias, A. B; Hall, H. K, Jr. *Macromolecules* **2001**, *34*, 5457–5462. (b) Sun, Z. C.; Jing, X. B.; Wang, X. H.; Li, J.; Wang, F. S. *Synth. Met.* **2001**, *119*, 399–400. (c) Folch, S.; Régis, A.; Gruger, A.; Coloban, P. *Synth. Met.* **2000**, *110*, 219–227. (d) MacDiarmid, A. G.; Zhou, Y.; Feng, J. *Synth. Met.* **1999**, *100*, 131–140.

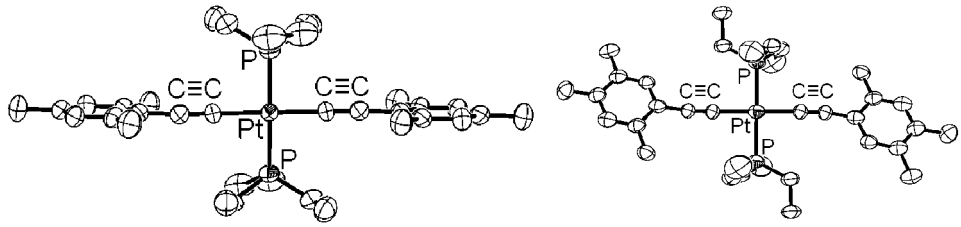

Figure 1. ORTEP representations of **1** (left) and **2** (right). The thermal ellipsoids are represented at 25% probability. The H atoms are not shown for clarity. Selected bond distances (Å) and angles (deg), **1**: Pt−P, 2.288(3); Pt−C, 2.013(9); C≡C, 1.184(13) ; PPtC, 91.3(3); **2**: Pt−P, 2.288(3); Pt−C, 2.047(10); C≡C, 1.148(12); PPtC, 90.6(3).

Scheme 1[a]

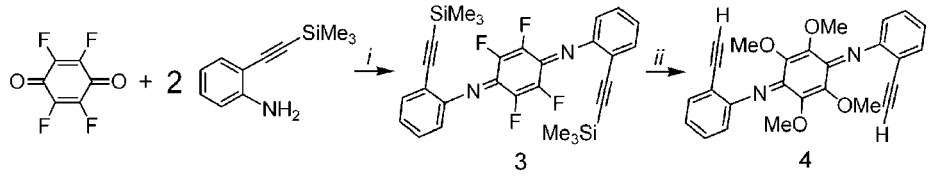

i = NEt_3, $TiCl_4$, C_6H_5Cl; *ii* = K_2CO_3, CH_3OH

[a] Only the *anti*-geometry is shown for simplicity.

may be the cause for this. A deviation of 6.9° from linearity of the C≡C−C fragment is also noted, corroborating this hypothesis. The variability in dihedral angle is not uncommon according to the Cambridge Data Bank. Examples where the relative angle between the PtP_2C_2 plane and the aryl group is nil or almost nil,[8] perpendicular or almost perpendicular,[9] or anywhere in between[10] are frequent. In these models, the δ value is about 15 ppm and the $J(^{31}P-^{195}Pt)$ coupling constant approaches 2400 Hz.

The synthesis of ligand **4** proceeds as indicated in Scheme 1. The precursor **3** is prepared from the condensation of a desired tetrasubstituted quinone with an *ortho*-substituted ethynyl(trimethylsilane)aniline. The structure determination of **3** was made by X-ray techniques (Figure 2; top) and reveals the *anti*-geometry (**3a**). Although several X-ray structures of *trans*-quinone diphenylimines were reported,[11] compound **3a** represents the first example of an *ortho*-substituted derivative. In Scheme 1, only the corresponding *anti*-conformer is presented for simplicity. After the next synthetic step (i.e., C−Si bond cleavage), the X-ray structure for the *syn*-conformer (**4b**) was also solved, demonstrating the existence of both conformers, the *anti* and *syn*. The angles between the phenyl rings and the central quinone average planes are 67.00° for the tetrafluoro-spacer (*anti*-conformer) and 88.89° for the tetramethoxy-spacer (*syn*-conformer), indicating that in both solids the π-systems are not well oriented for conjugation.

The thin-layer chromatography plates exhibit two spots for **3** and **4**, making a figure "8", most likely for the *anti*- and *syn*-conformers. These species were unfortunately not separable by column chromatography despite several attempts.

The C−Si bond cleavage by a base in methanol (i.e., methanolate) is accompanied by the substitution of all the fluoride atoms by methoxy groups, leading to **4**, for which an X-ray structure determination was made (Figure 2a). As stated in this particular case, the *syn*-conformation (**4b**) was observed. The incorporation of ethoxy substituents instead of methoxy was also tested (compound **4′**; Chart 4, and the obtained corresponding *ortho*-derivative was characterized by X-ray techniques (Figure 3), see Supporting Information for experimental). For **4′**, the *anti*-conformer was observed. The angle between the phenyl and quinone diimine average plane is 89.98°, almost completely perpendicular precluding efficient electronic communication by conjugation. This convenient reaction (C−Si bond cleavage and F-substitution by RO groups) was attempted

(8) (a) Ravera, M.; D'Amato, R.; Guerri, A. *J. Organomet. Chem.* **2005**, *690*, 2376–2380. (b) Schull, T. L.; Kushmerick, J. G.; Patterson, C. H.; George, C.; Moore, M. H.; Pollack, S. K.; Shashidhar, R. *J. Am. Chem. Soc.* **2003**, *125*, 3202–3203. (c) D'Amato, R.; Furlani, A.; Colapietro, M.; Portalone, G.; Casalboni, M.; Falconieri, M.; Russo, M. V. *J. Organomet. Chem.* **2001**, *627*, 13–22. (d) Long, N. J.; White, A. J. P.; Williams, D. J.; Younus, M. *J. Organomet. Chem.* **2002**, *649*, 94–99.

(9) (a) Mayor, M.; von Hanisch, C.; Weber, H. B.; Reichert, J.; Beckmann, D. *Angew. Chem., Int. Ed.* **2002**, *41*, 1183–1186. (b) Cooper, T. M.; Hall, B. C.; McLean, D. G.; Rogers, J. E.; Burke, A. R.; Turnbull, K.; Weisner, A.; Fratini, A.; Liu, Y.; Schanze, K. S. *J. Phys. Chem. A* **2005**, *109*, 999–1007. (c) Wong, W.-Y.; Ho, K.-Y.; Choi, K.-H. *J. Organomet. Chem.* **2003**, *670*, 17–26. (d) Wong, W.-Y.; Ho, K.-Y.; Ho, S.-L.; Lin, Z *J. Organomet. Chem.* **2003**, *683*, 341–353. (e) Schull, T. L.; Kushmerick, J. G.; Patterson, C. H.; George, C.; Moore, M. H.; Pollack, S. K.; Shashidhar, R. *J. Am. Chem. Soc.* **2003**, *125*, 3202–3203.

(10) (a) Jones, S. C.; Coropceanu, V.; Barlow, S.; Kinnibrugh, T.; Timofeeva, T.; Bredas, J.-L.; Marder, S. R. *J. Am. Chem. Soc.* **2004**, *126*, 11782–11783. (b) Deeming, A. J.; Hogarth, G.; Lee, M.-y.; Saha, M.; Redmond, S. P.; Phetmung, H.; Orpen, A. G. *Inorg. Chim. Acta* **2000**, *309*, 109–122. (c) Khan, M. S.; Al-Saadi, R. K. M.; Male, L.; Raithby, P. R.; Bjernemose, J. *Acta Crystallogr., Sect. E: Struct. Rep. Online* **2003**, *59*, m774–m776. (d) Stroh, C.; Mayor, M.; von Hanisch, C.; Turek, P. *Chem. Commun.* **2004**, 2050–2051. (e) Khan, M. S.; Al-Mandhary, M. R. A.; Al-Suti, M. K.; Ahrens, B.; Mahon, M. F.; Male, L.; Raithby, P. R.; Boothby, C. E.; Kohler, A. *J. Chem. Soc., Dalton Trans.* **2003**, 74–84. (f) Haskins-Glusac, K.; Ghiviriga, I.; Abboud, K. A.; Schanze, K. S. *J. Phys. Chem. B* **2004**, *108*, 4969–4978. (g) Wong, W.-Y.; Lu, G.-L.; Ng, K.-F.; Choi, K.-H.; Lin, Z. *J. Chem. Soc., Dalton Trans.* **2001**, 3250–3260. (h) Marsh, R. E. *Acta Crystallogr., Sect. B: Struct. Sci.* **2005**, *61*, 359–359. (i) Campbell, K.; McDonald, R.; Ferguson, M. J.; Tykwinski, R. R. *J. Organomet. Chem.* **2003**, *683*, 379–387. (j) Carpenter, J. P.; Lukehart, C. M. *Inorg. Chim. Acta* **1991**, *190*, 7–10. (k) Schmittel, M.; Kalsani, V.; Bats, J. W. *Inorg. Chem.* **2005**, *44*, 4115–4117. (l) Adams, C. J.; Bowen, L. E. *J. Chem. Soc., Dalton Trans.* **2005**, 2239–2240. (m) Davy, J.; Gunter, M. E.; Tiekink, E. R. T. *Z. Kristallogr.* **1998**, *213*, 483–486. (n) Bruce, M. I.; Davy, J.; Hall, B. C.; van Galen, Y. J.; Skelton, B. W.; White, A. H. *Appl. Organomet. Chem.* **2002**, *16*, 559–568. (o) Li, Q.-S.; Xu, F.-B.; Cui, D.-J.; Yu, K.; Zeng, X.-S.; Leng, X.-B.; Song, H.-B.; Zhang, Z.-Z. *J. Chem. Soc., Dalton Trans.* **2003**, 1551–1557. (p) Harriman, A.; Hissler, M.; Ziessel, R.; De Cian, A.; Fisher, J. *J. Chem. Soc., Dalton Trans.* **1995**, 4067–4080.

(11) (a) Gawlicka-Chruszcz, A.; Stadnicka, K. *Acta Crystallogr., Sect. C: Cryst. Struct. Commun.* **2002**, *58*, o416–o420. (b) Boone, H. W.; Bryce, J.; Lindgren, T.; Padias, A. B.; Hall, H. K., Jr *Macromolecules* **1997**, *30*, 2797–2799. (c) Blake, A. J.; Hubberstey, P.; Quinlan, D. J. *Acta Crystallogr., Sect. C: Cryst. Struct. Commun.* **1996**, *52*, 1774–1776. (d) Povet'eva, Z. P.; Chetkina, L. A.; Kopilov, V. V. *Zh. Strukt. Khim.* **1980**, *21*, 118–122.

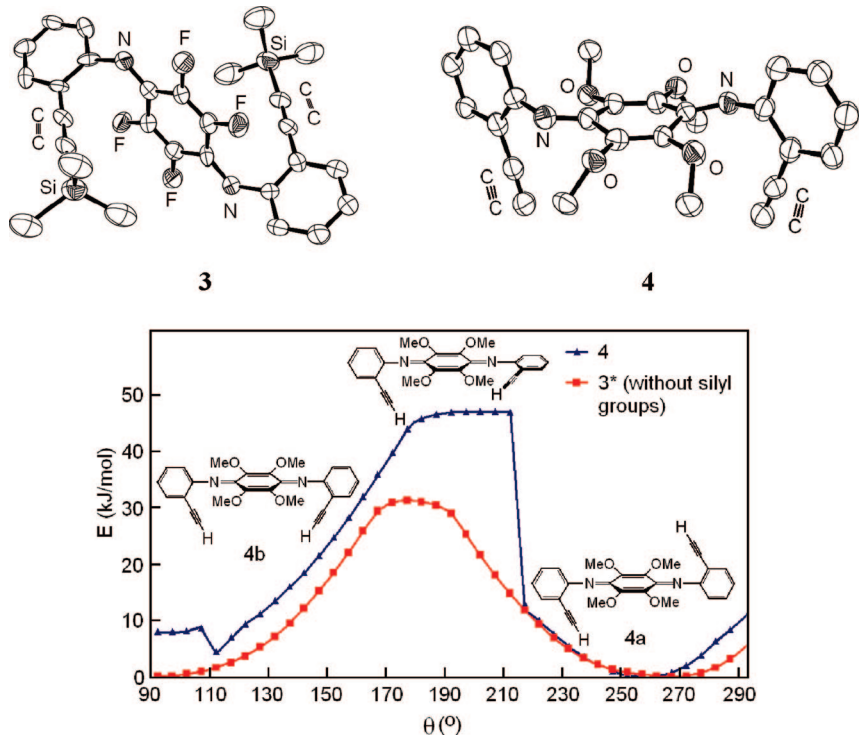

Figure 2. (Top) ORTEP representations of **3** (left) and **4** (right). The thermal ellipsoids are represented at 25% probability. The H-atoms are not shown for clarity. Selected bond distances (Å), **3**: C≡C, 1.204(5), C═N, 1.399(14); **4**: C≡C, 1.181(13), C═N, 1.273(9). (Bottom) Redundant relaxed energy scan at the Hartree–Fock level for **3*** (without silyl groups) and **4**. In these calculations, one-half of the molecule is fixed and the second half undergoes rotation about the N−Ph bond (θ = 90° at first).

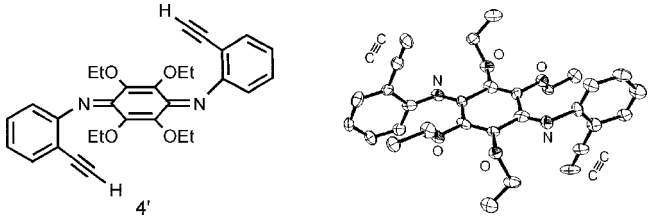

Figure 3. ORTEP representations of **4′** (right) and the corresponding Chemdraw (left). The thermal ellipsoids are represented at 25% probability. The H atoms are not shown for clarity. Selected bond distances (Å): C≡C, 1.187(13), C═N, 1.269(11).

Chart 4

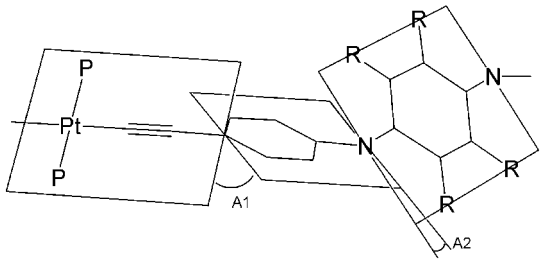

to test the facile incorporation of solubilizing chains often desired for polymers (polymer growth during synthesis, solubility for characterization, and protecting groups to minimize interchain interactions in the solid).

The difficulty in separating the *anti*- to *syn*-conformers is now addressed. Molecular modeling calculations on **4** as well as on **3*** (without the silyl groups) were performed to evaluate the energy barrier for the *anti*- to *syn*-conformer interconversion. The computational results are provided in Figure 2 (bottom). The calculations predict that the two conformers exhibit almost the same stability, consistent with the fact that both forms were observed from X-ray structure determination. The graph exhibits an energy barrier of 31 kJ/mol for **3*** (without silyl groups), a barrier small enough to observe fluxion at room temperature in solution. For **4**, a barrier of 47 kJ/mol is computed, a larger value stressing evidence for steric hindrance of the −C≡CH with the OMe groups. Noteworthy, the energy profile does not exhibit a Gaussian-shaped curve as observed for the fluoride-based ligand **3*** because of a cooperative action between one of the OMe groups and the $C_6H_4C{\equiv}CH$ group upon rotation. At a critical angle, the energy drops drastically after the MeO groups get "out of the way". These computations indicate that the barriers to fluxion are low enough to anticipate fluxion in solution. Maybe for this reason also, the separation of the *syn*- from the *anti*-forms was not possible in this work.

Ligands **5** and **6** were also prepared in the same manner as for **3** and **4** (Scheme 2). Both compounds were characterized by X-ray techniques (Figure 4). These structures reveal the *anti*-conformation in both cases and exhibit angles between the phenyl and quinone diimine mean planes of 55.15° and 69.38° for **5** and **6**, respectively. The smaller interplanar angles indicate that there is less steric hindrance and so less "torsion" on the π-system in comparison with the *ortho*-substituted species. These X-ray data also reveal that the fluoride substituents induce even less torsion than the methoxy groups.

Imine formation in **3**–**6** and **4′** is evidenced by the shorter C═N distance (ranging from 1.23 to 1.31 Å; X-ray) and the presence of a broad UV–vis band in the 500–700 nm range, giving the red to purple color in these materials. This color is very diagnostic since the most probable side product is the corresponding reduced diamine, which is white.[12]

Scheme 2

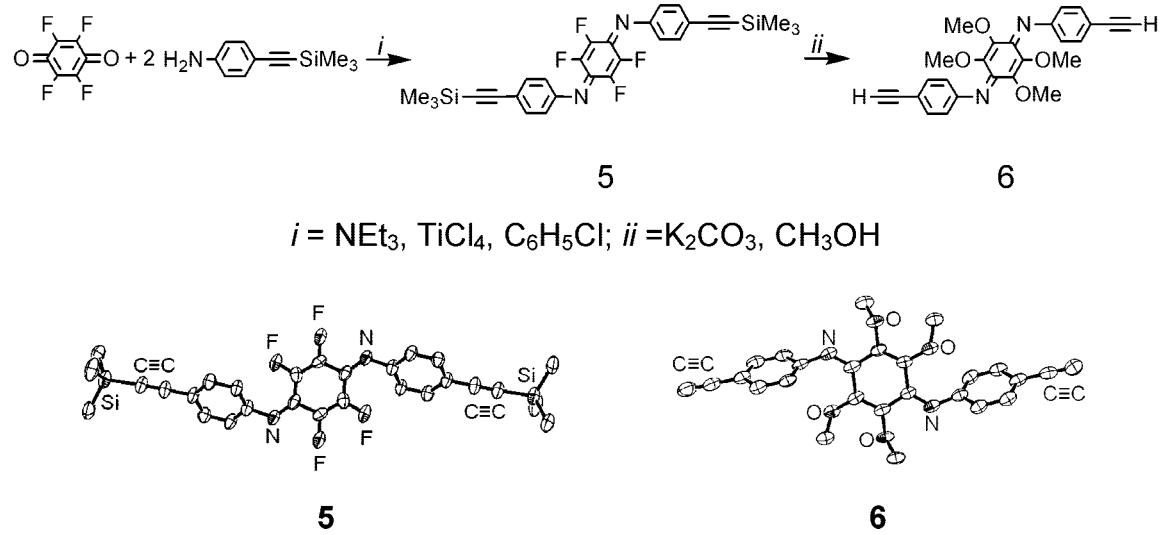

Figure 4. ORTEP representations of **5** (left) and **6** (right). The thermal ellipsoids are represented at 25% probability. The H atoms are not shown for clarity. Selected bond distances (Å); **5**: C≡C, 1.193(8), C═N, 1.296(9); **6**: C≡C, 1.190(8), C═N, 1.274(6).

Scheme 3

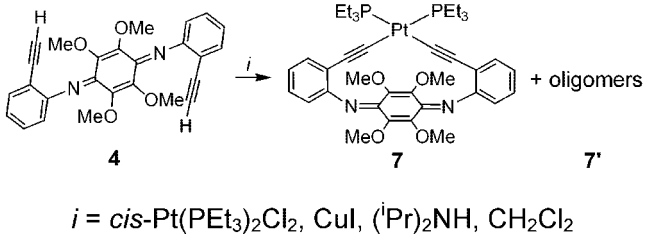

Synthesis of the Cyclic Model Compound 7 and Reaction with *cis*-Pd(PEt$_3$)$_2$Cl$_2$. **4** reacts with *cis*-Pt(PEt$_3$)$_2$Cl$_2$ in the presence of a base and CuI to form complex **7** and another small oligomer, **7′** (GPC), as verified by ^{31}P NMR of the crude product (Scheme 3).

After separation, complex **7** was characterized by X-ray crystallography (Figure 5). The starting Pt-containing complex in its *cis*-geometry turns out to be well adapted to coordinate *ortho*-ligand **4**, in its *syn*-conformation. This compound represents a rare example where the *cis*-geometry about the Pt(II) atom was used. Indeed, the *trans*-geometry is more often encountered (as indicated in refs 26 to 28), but some examples of *cis*-coordination also exist.[13] The presence of ring stress is noted in complex **7**, as evidenced by the deviation of the quinone diimine N═C$_6$(OMe)$_4$═N ring from planarity. The angle formed by the C═N axis and quinone diimine C$_6$-skeleton planes is 7.79°. The separable complex **7** (by column chromatography) also represents a model compound for *cis*-Pt-containing materials (polymers) readily identifiable from the ^{31}P NMR signature

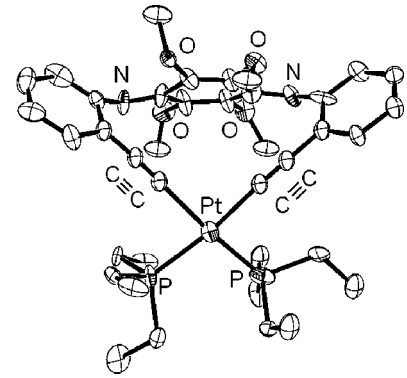

Figure 5. ORTEP representation **7**. The thermal ellipsoids are represented at 25% probability. H atoms are not shown for clarity. Selected bond distances (Å) and angles (deg): Pt−C, 1.928(30), Pt−P, 2.308(13), C≡C, 1.31(4), C═N, 1.27(5); PPtC = 87.2(9).

(δ = 8.7 ppm and $^1J(^{31}P-^{195}Pt)$ = 2225 Hz (in CD_2Cl_2)). The π-plane angle between the quinone diimine and phenyl rings is 61.40°. GPC indicated that the separated oligomers were primarily composed of very small oligomers of 2 and 3 units long.

The oligomers may also consist of a mixture of compounds with *anti*- and *syn*-ligands of the precursor,[11b] where the *anti*-form promotes polymerization, whereas the *syn*-form promotes the chelation. The presence of oligomers is also consistent with other literature works on Pt(II)-containing trimers, tetramers, and higher oligomers.[14,15]

Attempts were also made to generate Pd-containing complexes and polymers analogous to **7** and **7′**. *cis*-Pd(PEt$_3$)$_2$Cl$_2$ reacts with **4** in the presence of CuI with the possibility of C−C coupling occuring (Scheme 4). The compounds **8** and **9** were characterized by X-ray techniques (Figure 6), and other oligomers were also detected in the GPC traces (n = 2, 3).

Compound **8** is formed by C−C coupling as anticipated. The reaction mechanism should proceed through a Pd-containing

(12) The corresponding diamines for ligand **3** (*cis* and *trans*) were isolated and characterized by X-ray crystallography as reaction side products. The crystals were colorless, the C═N distance ranging form 1.39 to 1.41 Å. The angles made by the peripheral aryls vs central aryl were 51.53° and 63.97° for the *trans*-conformer and 49.84° for the *syn*-conformer, respectively. This shows that crystal-packing forces could also participate in the π-torsion angles, since we find more than 10° torsion angle difference in a same crystal packing. However, in this case it is an amine instead of an imine bound to the quinone ring, allowing for free rotation on both sides of the nitrogen.

(13) (a) Johnson, C. A., Jr.; Baker, B. A.; Berryman, O. B.; Zakharov, L. N.; O'Connor, M. J.; Haley, M. M. *J. Organomet. Chem.* **2006**, *691*, 413–421. (b) Johnson, C. A., Jr.; Haley, M. M.; Rather, E.; Han, F.; Weakley, T. J. R. *Organometallics* **2005**, *24*, 1161–1172.

(14) Vincente, J.; Chicote, M.-T.; Alvarez-Falcon, M. M.; Jones, P. G. *Chem. Commun.* **2004**, 2658–2659.

(15) Lee, S. J.; Luman, C. R.; Castellano, F. N.; Lin, W. *Chem. Commun.* **2003**, 2124–2125.

Scheme 4

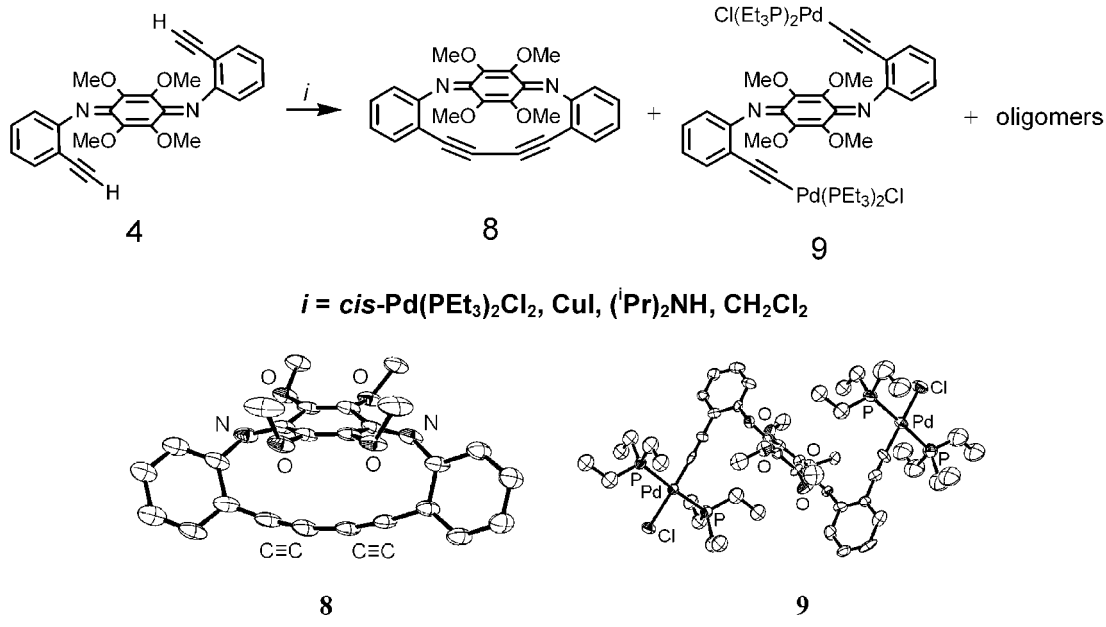

Figure 6. ORTEP representations of **8** (left) and **9** (right). The thermal ellipsoids are represented at 25% probability. The H atoms are not shown for clarity. Selected bond distances (Å) and angles (deg), **8**: C≡C, 1.204(8), C═N, 1.278(6); **9**: Pd−P, 2.297(6); Pd−Cl, 2.341(6), C≡C, 1.204(8), C═N, 1.278(6); PPdCl, 89.3(2), PPdC, 92.0.

Scheme 5

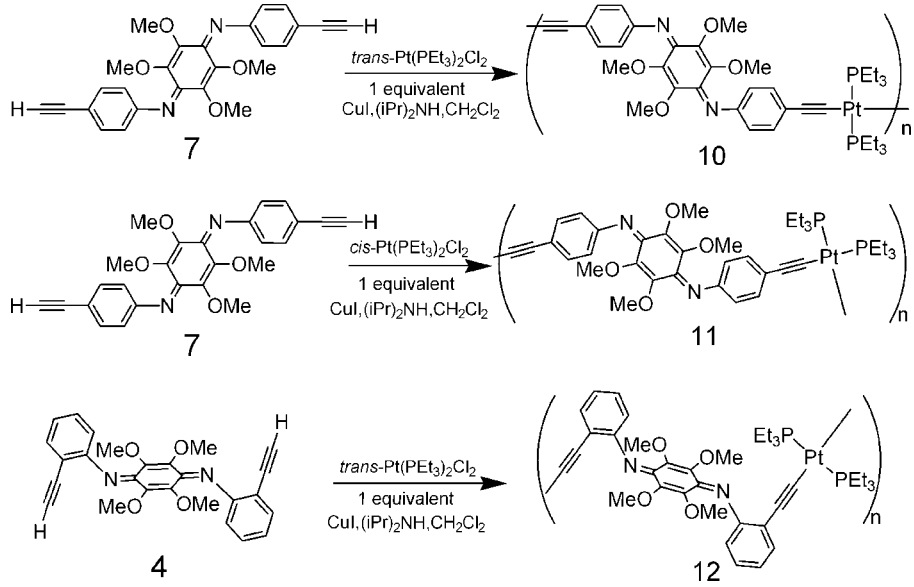

precursor with a structure similar to that of **7**, where the macrocycle exhibits the appropriate *cis*-orientation for C−C coupling. It is reasonably anticipated that the existence of this macrocycle precursor stems from ligand **4b** (*syn*-conformer) and *cis*-$Pd(PEt_3)_2Cl_2$. Moreover, the characterization of compound **8** corroborates the presence of the *syn*-conformer for spacer **4**, while the *anti*-conformer is evidenced by the structure of the binuclear complex **9**. The latter complex is interesting because a *cis/trans* isomerization took place, which is rare but not unprecedented.[16] This isomerization was not observed for the Pt-containing materials. Interestingly, **9** also represents a model for the Pt-containing polymers built upon an *ortho*-substituted spacer and a *trans*-metallic fragment (noted as *ortho/trans*). On the basis of this structure, the synthesis of *ortho/trans* polymers is possible from the extension at the chloro positions.

For **9**, the interplanar angle between the phenyl and quinone planes is 84.78°. The imine functions are also evidenced by the short N═C distances (1.28 Å). This rather large angle (~85°) makes conjugation difficult through the π-orbitals. The angle made by the aryl and the $Pt(PEt_3)_2(CC)_2$ planes is 81.47°.

Syntheses of the Oligomers and Polymers. The syntheses of polymers **10**−**12** proceed the same way as mentioned for **7** (Scheme 5). The nature of the coordination geometry about the Pt atom is confirmed by ^{31}P NMR by comparison with the diagnostic chemical shifts of the model compounds **1** and **2** for polymers **10** and **12** (δ is in the 15 ppm range) and compound **7** for polymer **11** (δ is in the 8.5 ppm range). Similarly, the 1:1 ratio of ligand and Pt-containing starting material in the

(16) Cross, R. J.; Davidson, M. F. *Inorg. Chim. Acta* **1985**, *97*, L35–L36.

Table 1. Molecular Weight Determination of the Polymers 10–12[a]

polymer	M_n[c]	M_w	PD
10[b]	32 400 (38)	68400	2.1
11[b]	16 800 (20)	17300	1.0
12[b]	6600 (8)	10000	1.5
7′[d]	3600 (4)	4400	1.2

[a] GPC against monodispersed polystyrene standards. [b] Measured after fractionation, which consisted of precipitation by diethyl ether. [c] The values in brackets are the average number of units in the chain obtained by dividing M_n by the molecular weight of a repetitive unit. [d] Portion separated from the reaction presented in Scheme 3 by column chromatography.

polymers is confirmed by ^{1}H NMR (using the integrated signals for Me vs Et). Stand-alone films were obtained for **10** (SI) and **11**. The striking feature is the polydispersity of the crude polymers based on the GPC traces, in which small oligomers all the way to large polymers are detected, notably for **10** and **11**. Fractionation is performed by precipitating the polymers **10**–**12** out of a concentrated CH_2Cl_2 solution using diethyl ether as the poor solvent. For comparison purposes, the fractions of oligomers separated for the reaction of Scheme 3, which are noted as "oligomer **7′** (*anti-ortho-cis*)", were also investigated. These oligomers and precipitated polymers **10**–**12** exhibited M_n ranging from 3600 to 32 400 (Table 1). From this analysis, we observe that the molecular weight has a tendency to get higher with more linear building-block ligands. The trend is that both M_n and M_w vary as *cis* < *trans* and *ortho* < *para* and may reflect the steric hindrance and geometry twist effects. Also, this steric hindrance may slow the growth process of the polymer. No attempt was made to increase the M_n, M_w, and PD parameters, as this was not the purpose of this work.

The thermal stability was >300 °C in all 3 cases (SI), whereas the small oligomers (primarily composed of dimers and trimers separated from compound **7** using column chromatography) exhibited weight loss between 100 and 200 °C. For polymers **10** and **11**, a glass transition was detected at ∼147 °C (SI) and at 142 °C, respectively.

Electrochemical Oxidation Properties of the Oligomers and Polymers. *N*,*N*′-Diphenylquinone diimine exhibits oxidation processes in its protonated form only.[6b–d,17,18] PhC≡CH exhibits an irreversible, large oxidation wave in the CVs (cyclic voltammograms; 1.5−2.0 V vs Ag/AgCl).[19] This irreversibility is due to the presence of a radical-type polymerization process forming polyphenylacetylene.[19] The CV of the ligands, model compounds, and polymers (SI) and the observed oxidation and reduction peaks are reported in Table 2. The CV of *trans*-PhC≡CPt(PEt$_3$)$_2$C≡CPh was also studied and compared well with the literature.[20,21] This compound exhibits an irreversible oxidation peak at ∼1.2 V vs Ag/AgCl, and 1.43 ± 0.21 electron was transferred in a benzene/acetonitrile mixture.[21] This irreversible oxidation peak was also observed by us at 1.17 V vs SCE in acetonitrile (+0.1 M TBAPF$_6$) with 1.1 ± 0.2 transferred electron. We do not have an explanation for this small difference except that a weak irreversible peak was also noted at 0.97 V vs SCE (also seen in the other samples) corresponding to about 0.2 electron based upon a comparison of the peak height. The purity was checked by ^{1}H NMR. A chemically reversible but electrochemically irreversible reduction wave was also noted. The cathodic and anodic peaks for this reduction process are very broad.

The CVs for **1** and **2** show a series of irreversible oxidation peaks in the same window as for *trans*-PhC≡CPt(PEt$_3$)$_2$C≡CPh, but two differences are observed. First, the number of peaks increased in the 1–1.5 V window, and the peaks are shifted to lower potentials. Both observations are due to the methyl group donating inductive effect, rendering the phenyl groups easier to oxidize. This is well exemplified by the shift of the 1.17 V peak (of *trans*-PhC≡CPt(PEt$_3$)$_2$C≡CPh) down to 1.11 and 1.06 V vs SCE for **1** and **2**, respectively. The presence of peaks at 1.42 and 1.46 V for **1** and **2** may also arise from a shift of a higher potential peak (presumably above the 1.5 V limit used for the comparison molecule, *trans*-PhC≡CPt(PEt$_3$)$_2$C≡CPh). Coulometry for **2** reveals that the number of transferred electrons is 1.1, 1.4, and 1.1 ± 0.2 for the peaks located at 1.06, 1.46, and 1.70 V, respectively, consistent with their relative height and that observed for *trans*-PhC≡CPt(PEt$_3$)$_2$C≡CPh. **1** and **2** exhibit broad and ill-defined irreversible reduction peaks. Fractional numbers of transferred electrons were also noted for the reductions and were not studied further. All in all, **1** and **2** exhibit multiple irreversible waves in the 0.9–1.82 V range and are used for assignment purposes with the polymers.

The bis(ethynylbenzene)quinone diimine compounds **3** and **5** exhibit two sets of reduction waves only in the −0.37 to −1.20 V range. The peaks of **3** are found irreversible. For **5**, the peak at −0.48 V appears reversible. The peak at −0.96 V shows a very slow electron transfer. Hence, these model compounds exhibit low potential reduction peaks, totally consistent with the assignment for being an electron acceptor.

Compound **7** exhibits three irreversible peaks resembling that of **1** and **2**, allowing one to assign the oxidation to the PhC≡CPt(PEt$_3$)$_2$C≡CPh unit. A quantity of 1.0 ± 0.2 for both peaks at 1.00 and 1.42 V are transferred, again consistent with the findings for **1** and **2**. Polymers **10**−**12** exhibit two or three peaks on the oxidation side, but the signals are ill-defined and located at lower potentials, consistent with an extended conjugated polymer where the wave widths are associated with polydispersity. Compound **7** and polymer **11** exhibit irreversible ill-defined reduction peaks and were not investigated further.

Analysis of the Frontier Orbitals and UV–Vis Spectra. An earlier report on the bimolecular charge transfer interactions between 7,7,8,8-tetracyanoquinodimethane (TCNQ) and a series of *trans*-Pt(PR$_3$)$_2$(C≡CR′)$_2$ complexes (R = Me, Et, Pr, Bu; R′ = H, CH$_2$=CH, MeC≡C, Ph) exists.[22] The purple 1:1 adducts exhibit an absorption in the 506–555 nm range in the UV–vis spectra similar to our polymers. The authors deduced that the electron was donated from the alkynyl fragment to the TCNQ unit. These findings provide interesting clues for the investigated systems.

The UV–vis spectra and MO descriptions (DFT and TDDFT) of the parent compounds *trans*-PhC≡CPt(PR$_3$)$_2$C≡CPh (R = Et, Bu, Ph) to the models **1** and **2** were previously studied throughout the literature.[4k,23–25] Only a brief account of the relevant information is provided below. The complexes exhibit

(17) Ueda, F.; Mikai, K.; Harada, I.; Nakajima, T.; Kawagoe, T *Macromolecules* **1990**, *23*, 4925–4928.
(18) Turovska, B.; Stradins, J.; Glezer, V.; Lokmane, E.; Sarule, E.; Freimanis, J. *Zinatnu Akademijas Vestis, Kimijas Serija* **1989**, 108–15.
(19) Garcia-Canadas, J.; Lafuente, A.; Rodriguez, G.; Marcos, M. L.; Gonzalez Velasco, J. *J. Electroanal. Chem.* **2004**, *565*, 57–64.
(20) Kershman, J. R.; Paris, K. E.; Stamey, J. A.; Pyati, R *J. Electroanal. Chem.* **2006**, *597*, 87–94.
(21) Kondrachova, L.; Paris, K. E.; Sanchez, P. C.; Vega, A. M.; Pyati, R.; Rithner, C. D. *J. Electroanal. Chem.* **2005**, *756*, 287–294.
(22) Masai, H.; Sonogashira, K.; Hagihara, N. *J. Organomet. Chem.* **1972**, *34*, 397–404.
(23) Wong, C.-Y.; Che, C.-M.; Chan, M. C. W.; Han, J.; Leung, K.-H.; Philips, D. L.; Wong, K.-Y.; Zhu, N. *J. Am. Chem. Soc.* **2005**, *127*, 13997–14007.
(24) Batista, E. R.; Martin, R. L. *J. Phys. Chem. A* **2005**, *109*, 9856–9859.

Table 2. Observed Electrochemical Waves[a]

compound	oxidation	reduction
trans-Ph-C≡C-PtEt_2-C'C-Ph	0.97 (ir), 1.17 (ir)	−0.62/−1.06[b]
1	∼1.0 (ir), 1.11 (ir) 1.42 (ir), 1.82 (ir)	−0.32 (ir), −1.74 (ir)
2	0.90 (ir), 1.06 (ir) 1.46 (ir), 1.70 (ir)	−1.09 (ir)
3	1.06 (ir) weak	−0.58 (ir), −1.15/-1.09
5		−0.58/−0.37[b], −1.20/−0.72[b]
7	0.77 (ir) 1.00 (ir), 1.42/1.25[b]	
10	0.67 (ir), 1.16/1.01[b]	
11	0.60 (ir), 0.96 (ir), 1.26 (ir)	
12	0.51 (ir), 0.68 (ir), 1.12 (ir)	−1.06 (ir.)

[a] Volts vs SCE; ir = irreversible (i.e., no return wave). [b] Electrochemically irreversible as the difference between the anodic and cathodic waves exceeds 60 mV.

strong lowest energy absorption bands between 320 and 340 nm. For example, for R = Ph, these are found at 330 (sh; ϵ = 43 600) and 337 nm (ϵ = 44 900 M^{-1} cm^{-1}).[23] Reported DFT results (B3LYP) for *trans*-PhC≡CPt(PBu_3)$_2$C≡CPh indicated that the HOMO is composed of conjugated π-orbitals, which include contribution from the Pt(d_{xy}) orbital, while the LUMO consists of the ligand π^* orbitals only.[4k] Thus the lowest energy excitation is a mixture of $\pi\pi^*$ and MLCT (metal-to-ligand charge transfer). This assignment is corroborated by the difference in band shape between the complex (broad) and the free ligand (as PhC≡CH; narrow absorption). However, a recent computational report (TDDFT) pointed out that this first excitation is a mixture between two contributions, which are $\pi\pi^*$ (59%), similar to that described above (i.e., with a MLCT character), and LMCT (32%; also primarily $\pi\pi^*$). These two transitions arise from two different vertical but nearly degenerated excitations (difference only 0.04 eV; $\varphi_g \rightarrow \varphi_u^*$ and $\varphi_u \rightarrow \varphi_g^*$, where φ_g and φ_u and φ_g^* and φ_u^* are π- and π^*-orbitals, respectively, and the "g" orbitals include the Pt(d_{xy}) orbital). This more recent analysis better corroborates our results and our experimental observations for **1** and **2**. It is not clear whether the strong absorptions are MLCT or LMCT since the LUMO implies the complete molecules including the ligands and the metal.

The nature of the frontier MOs is addressed by DFT, and the transition energies and oscillator strength are addressed by TDDFT. The crystal structure data of **1**, **2**, **4**, **6**, and **7** were used as input files for all calculations. The frontier MO drawings are shown in Figure 7.

The HOMO for **1** and **2** exhibits atomic contributions spreading from the aryl π-system to the π-systems of the ethynyls to the Pt d-orbitals. However the LUMOs for **1** and **2** differ greatly. For **1**, the electronic density is primarily concentrated about the Pt d and π C≡C with almost no contribution on the mesityl residue. Conversely, the LUMO for **2** exhibit an electronic density spreading from the Pt d-orbitals to the π-system of the aryl group, indicating a longer electronic delocalization. All in all, the orientation of the aryl groups with respect to the $PtP_2(C{\equiv}C)_2$ plane (83.0° for **1** and 29.8° for **2** defined as A1 in Chart 4) clearly plays an important role in the nature of the LUMO. Figure 7 also shows representations for the relevant HOMO−1 and HOMO−2 for **1**. The HOMO−1 is composed of the π-system of the ethynylaryl fragments with some contribution of the lone pair of the P atoms. No contribution is computed for the Pt metal. The HOMO−2 is composed primarily of the π-systems of the ethynyl linkers and the Pt d-orbitals.

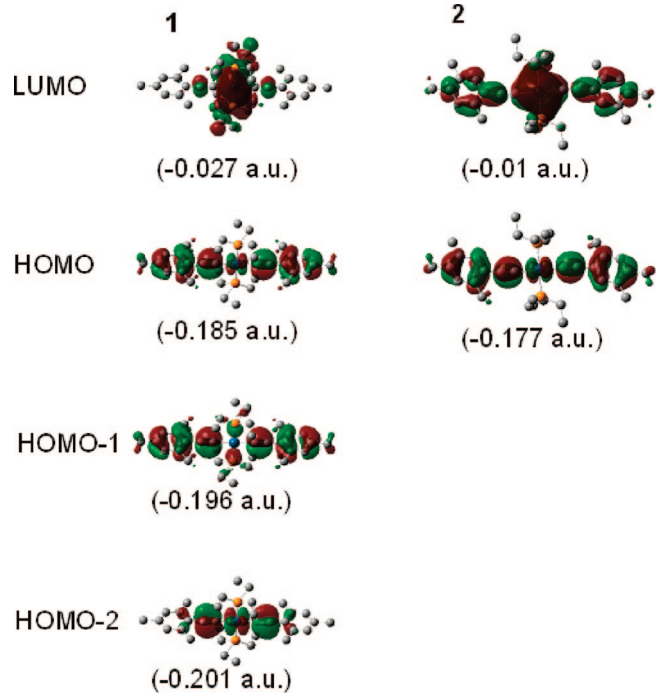

Figure 7. Representations of the relevant frontier MOs for **1** and **2**.

Table 3. UV−Vis Data for Model Compounds and Polymers 10–12[a]

compound or polymer	λ_{max} in nm (ε in M^{-1} cm^{-1})
1	270 (43 600), 312 (sh), 322 (20 000)
2	266 (154 000), 286 (sh), 330 (118 000)
4	240 (38 800), 318 (48 500), 476 (3440)
6	260 (23 400), 320 (38 900), 480 (4200)
7	266 (25 381), 314 (41 200), 514 (2100)
7′	240 (38 300), 310 (40 000), 510 (2500)
10	350 (59 300), 560 (13 700)
11	330 (28 300), 540 (5900)
12	265 (28 000), 314 (40 200), 535 (2700)

[a] In 2 MeTHF at 298 K.

Four electronic transitions are possible from the MOs presented in Figure 7 (3 for compound **1** and 1 for compound **2**). These are all MLCT transitions, consistent with previous finding for the *trans*-PhC≡CPt(PBu_3)$_2$C≡CPh complex. The computed oscillator strength for the HOMO → LUMO transition for **2** is 0.70, and the calculated wavelength is 314 nm (the experimental value is 330 nm (ϵ = 118 000 M^{-1} cm^{-1}); Table 3). In **1**, the HOMO → LUMO transition exhibits an oscillator strength of 0.02, meaning that this contribution to the intensity is minimal. On the other hand, the HOMO−2 → LUMO transition exhibits a calculated oscillator strength of 0.13 and a

(25) Cooper, T. M.; Krein, D. M.; Burke, A. R.; McLean, D. G.; Rogers, J. E.; Stagle, J. E. *J. Phys. Chem. A* **2006**, *110*, 13370–13378.

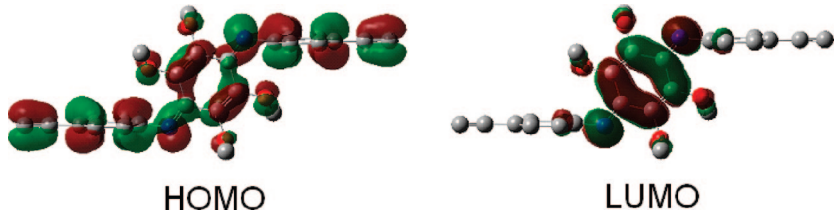

Figure 8. HOMO and LUMO for ligand **6** (methyl groups not shown).

wavelength of 314 nm (the experimental value is 322 nm (ϵ = 20 000 M^{-1} cm^{-1})). The relative amplitude of the oscillator strengths for **1** and **2** corroborates well the observed absorptivities. These computations, again, stressed the importance of the angle made by the aryl group and the $PtP_2(C{\equiv}C)_2$ planes (A1). For comparison purposes, the geometry optimizations of **1** and **2** were performed and the positions of the associated MLCT bands were calculated (SI). The calculated A1 and λ_{max} are 73.9° and 61.7° and 327 and 331 nm for **1** and **2**, respectively. Despite the large change in A1 value (29.8° (X-ray) vs 61.7° (optimized geometry)) for **2**, these red-shifted calculated λ_{max} values still agree with the experimentals (327 vs 322 for **1** and 331 vs 330 nm for **2**), illustrating the good electronic "communication" of the ethynyl bridge.

The *para*-substituted ligand **6** was analyzed by TDDFT (using the available X-ray data) as a representative example of the isolated ligand, and the frontier MOs are shown in Figure 8. The HOMO is composed of all C(p_x) and N(p_x) atomic orbitals extending from one ethynyl residue to the other, with the exception of the methyl groups, stressing the obvious conjugation across the ligand, despite the angle of 69.4° made by the phenyl groups and the quinone diimine ring (defined as A2 in Chart 4). Conversely, the LUMO exhibits an enhanced electronic density over the quinone diimine segment and shows a decrease in atomic contribution on the ethynylphenyl side arms (i.e., practically nil). Hence, DFT calculations predict a lowest energy electronic transition corresponding to a charge transfer process (CT), ethynylphenyl → quinone diimine.

The computed HOMO → LUMO transition wavelength is 554.8 nm and compares reasonably with the observed low-energy band spreading from 400 to 600 nm (λ_{max} = 480 nm; ϵ = 4200 M^{-1} cm^{-1}). The computed oscillator strength is 0.09, suggesting that the electronic transition is of weak intensity, probably because of the 69.38° twist between the phenyl groups and the quinone diimine ring (A2). This observation corroborates well the observed low absorptivity (ϵ = 4200 M^{-1} cm^{-1}; Table 3). Two other absorptions are observed at 260 and 320 nm.

Prior to discussing the computational results for a model compound for polymer **10**, it is important to state that no X-ray data are available for any polymers. Instead, geometry optimization is necessary, and in order to make appropriate comparisons, the optimized geometry and TDDFT computations for **4**, **6**, and **7** were also performed (SI). All in all, some differences in geometry (angles A1 and A2 vary from 5° to 20°) as well as calculated 0–0 position and oscillator strengths are noted (SI). The general trend is that the computed 0–0 position is systematically red-shifted for the optimized geometry, but these 0–0 positions do not exceed the tail of the observed CT absorption nor induce a change in the observed relative trend. So, the CT assignment remains unchanged whether one uses the X-ray or optimized geometry for analysis. Similarly, the incorporation of solvent molecules (here THF instead of 2MeTHF) also induces a small red-shift of the calculated CT 0–0 positions (SI; 20 nm for **6** and 30 nm for **7**), but again these values fit with the experimental spectra in the sense that these values are located in the tail of the band.

The frontier MOs for the model compound *trans*-(ligand **6**)−Pt(PEt$_3$)$_2$−(ligand **6**) representing a segment of polymer **10** is investigated. The geometry of this model was first optimized prior to MO analysis (Figure 9). The angle A2 between the phenyl rings and quinone average plane is 49.75°, obviously deviating from coplanarity. This effect is induced by methoxy streric contacts with the phenyl groups. This angle is 10° less than that observed in the X-ray structure of the ligand alone (**6**). However, this angle is also much less (∼35°) than in the structure of model complex **9** (84.78°) built from an *ortho*-substituted ligand and supports the tendency stated above that the *ortho*-ligands induce more twist to the π-system than does the *para*-ligands. The angle A1 between the Pt(PEt$_3$)$_2$(C≡C)$_2$ plane and the phenyl rings in **9** is 81.47°, which is closer to model complex **1** (83.0°) than **2** (29.8°).

The frontier MOs are presented in Figure 9. The HOMO is composed of C(p_x) and N(p_x) atomic orbitals extending from one ethynyl residue to the other, including some Pt(d_{xy}) orbital, securing contact all across the chain, even though the planes deviate from planarity. This MO bears close similarities with those described above (i.e., φ_g and φ_u). The LUMO is composed of C(p_x) and N(p_x) primarily localized in the quinone diimine segment. Thus, the computed lowest energy transitions are also CT excitations (PhC≡CPt(PEt$_3$)$_2$C≡CPh → quinone diimine). The resemblance of the UV–vis spectra of ligands **4** and **6** with that of the polymers **10**−**12** and compound **7** strongly supports this assignment. TDDFT calculations predict that the 0–0 absorption is placed at 660 nm (with an oscillator strength of 2.10), which appears reasonable considering that the observed CT absorption spreads from 450 to 700 nm. Also, the computed oscillator strength appears a little more than 1 order of magnitude larger than that computed for **6** above (0.09). This observation is consistent with the effect of the angle A2 between the phenyl and quinone diimine average planes on the absorptivity (Table 4). For example, the angle A2 (49.8°) computed for the optimized *trans*-(ligand **6**)−Pt(PEt$_3$)$_2$−(ligand **6**) complex, representing a fragment of polymer **10**, is smaller than that observed for the compound **6** (X-ray; 69.4°). Experimentally, the measured absorptivity of the CT band of polymer **10** is ∼3-fold larger (13 700) than that found in ligand **6** (4200 M^{-1} cm^{-1}).

Complex **7** was also investigated by DFT methods using the X-ray data. The similarity in shape of the UV–vis spectra to the polymers and ligands strongly suggests that the lowest energy excited states are CT states as well. The MO representations for the frontier MOs, notably LUMO, HOMO−1, and HOMO, are available in the Supporting Information. Both filled orbitals exhibit the usual C(p_x) and N(p_x) contributions all across the conjugated loop. The HOMO also exhibits some Pt(d_{xy}) contributions, stressing the obvious similarity with the model compounds and ligand **6** computed above. The LUMO exhibits atomic contributions (also C(p_x) and N(p_x)) mainly localized

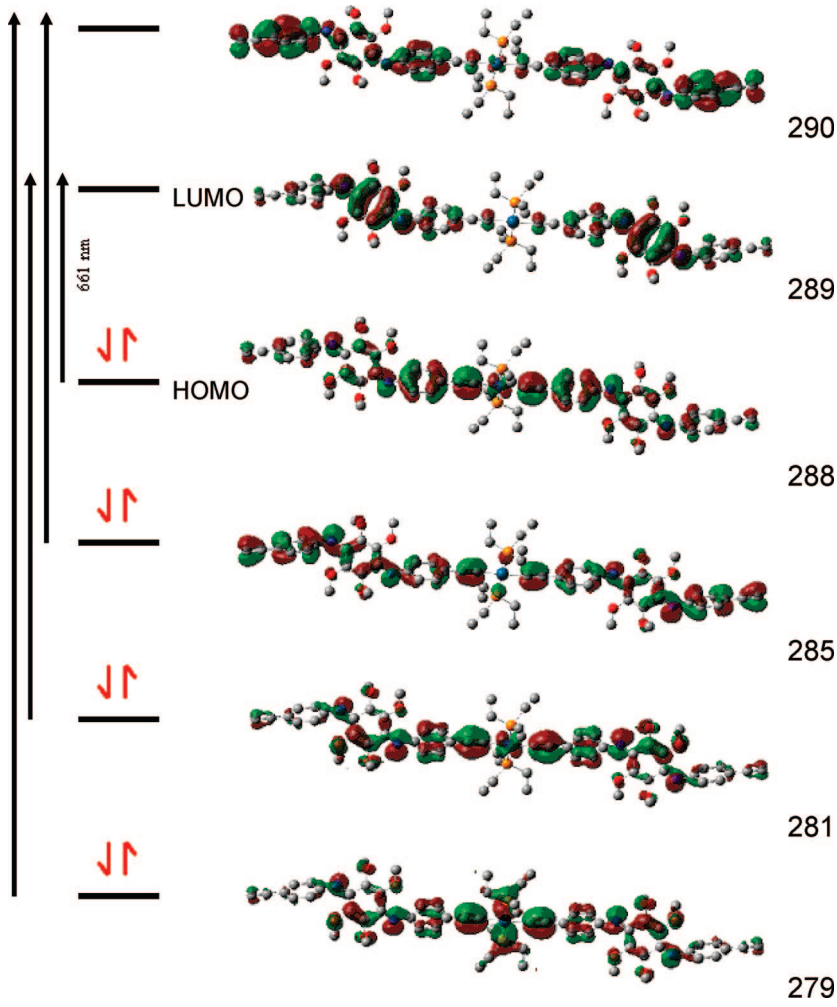

Figure 9. Frontier MOs for the model compound *trans*-(ligand **6**)−Pt(PEt_3)$_2$−(ligand **6**). The respective MO energies are from bottom to top: –0.181, –0.176, –0.097, –0.096 (degenerated), –0.018, –0.016 au, respectively.

Table 4. Comparison of the Calculated and Experimental Absorption Maximum with the Structural Parameters A1 and A2 Presented in Chart 4 Using X-ray Data, and Comparison of λ_{max} Absorption with the Molecular Weight[a]

compound or polymer	A2 (°)	A1 (°)	calcd 0–0 position in nm (oscillator strength) crystal geometry	exptl λ_{max} in nm (ε in M^{-1} cm^{-1})	nature of the excited state
1		83.0	314 (0.13)	322 (20 000)	MLCT
2		29.8	314 (0.70)	330 (118 000)	MLCT
4b	88.9		536 (0.0006) 516 (0.001) 412 (0.012)	476 (3440)	CT
6	69.4		539 (0.09) 524 (0.03) 442 (0.001)	480 (4200)	CT
7	61.4	67.9	551 (0.04) 483 (0.02)	514 (2100)	CT
10	49.8	82.7		560 (13 700)	CT

compound	M_w or M (g/mol)	λ_{max} absorption (nm)
4	426.5	476
6	426.5	480
7	4400	514
12	10 000	535
11	17 300	540
10	68 400	560

[a] All angles are from X-ray data, except for **10** (DFT; also see Supporting Information).

on the quinone diimine residue. Thus, the computed lowest energy excitation is also a CT transition despite the *cis*-geometry of the metal. In this case, the ring stress makes the parameter A2 (61.4°) less adequate for efficient CT process (i.e., less allowed) than polymer **10** for example. Indeed, TDDFT predicts that the HOMO → LUMO absorption band should be placed at 551 nm, a calculated value that is blue-shifted in comparison with that computed for **10** (660 nm). Moreover, a small oscillator strength of 0.04 is computed (in comparison with 2.1 for **10**). These comparisons corroborate the observed values (λ_{max} = 514 nm and ϵ = 2100 M^{-1} cm^{-1} for complex **7**, and λ_{max} = 560 nm and ϵ = 13 700 M^{-1} cm^{-1} for polymer **10**).

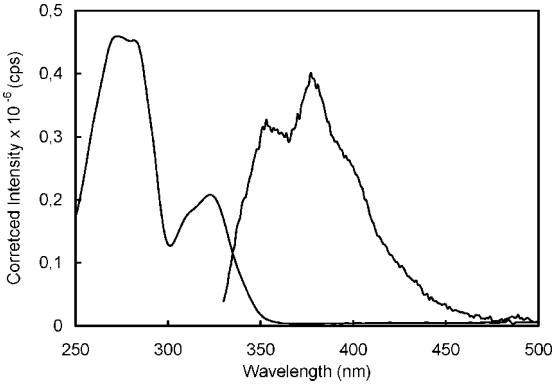

Figure 10. Fluorescence (right) and absorption spectra (left) of **2** in degassed 2MeTHF at 298 K. λ_{exc} = 322 nm.

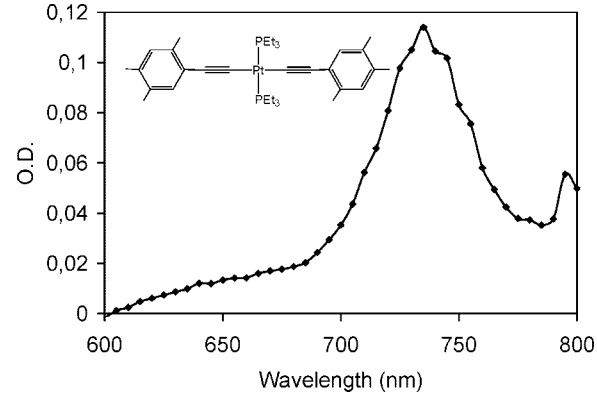

Figure 11. Transient absoption spectrum for **2** in 2MeTHF at 77 K in the 600–800 nm window recorded 150 μs after the laser pulse. The excitation wavelength is 355 nm.

The comparison of the λ_{max} going from spacers **4** and **6** to compound **7** to the oligomers and polymers **7′** and **10**−**12** reveals a trend. When the π-system extends, the absorption band is red-shifted. The trend follows that of the molecular weight (Tables 1 and 4b), **4** = **6** < **7** < **12** < **11**< **10** with λ_{max} = 476, 480, 514, 535, 540, 560 nm, respectively. This comparison demonstrates the conjugation along the polymer backbone. Moreover, the values of the absorption coefficient are clearly a function of the π-orbitals' alignment (parameters A1 for the MLCT and A2 for CT); the more aligned the π-orbitals, the more intense the absorption bands are. To our knowledge, such detailed analysis of the structural parameters of the polymer chain on the optical properties is unprecedented.

Photophysical Properties. For all compounds and polymers, no emission is detected in solution and in the solid state at 298 K, except for the compounds **1** and **2** and spacers **4** and **6**. On the other hand, all compounds and polymers except **10** exhibit luminescence in 2MeTHF at 77 K.

1. Model Compounds 1 and 2. The *trans*-PhC≡CPt(PBu$_3$)$_2$C≡CPh compound exhibits fluorescence with a 0–0 localized at 346 nm at room temperature in methylcyclohexane with a fluorescence quantum yield (Φ_F) < 0.0006.[4n] In this work, the weak fluorescence for this compound is also detected at the same spectral position using 2MeTHF as the solvent. Similarly, a weak fluorescence with a 0–0 peak at 356 nm was also detected for **2** in degassed 2MeTHF at 298 K (Figure 10). These two λ_{max} are blue-shifted with respect to Pt(dppe)(C≡C-*p*-C$_4$H$_4$R)$_2$ (λ_{max} = 450 nm; dppe = Ph$_2$PCH$_2$CH$_2$PPh$_2$; R = Me, C≡CH),[4g] which exhibit the dppe-directed *cis*-conformation. The fluorescence lifetime (τ_F) for **2** is <0.1 ns, the detection limit of our instrument, consistent with the weak intensity.

No phosphorescence is detected at 298 K for *trans*-PhC≡CPt(PBu$_3$)$_2$C≡CPh,[4n] **1** and **2**, but the triplet excited states can still be accessible from T_1-T_n absorption. For the former compound, the reported T_1-T_n band is located in the 400–650 nm range with a 0–0 peak placed at ~645 nm. The transient lifetime is 590 ± 150 ps.[4n] Our instrument limit (laser pulse width of 13 ns) did not allow us to reach this time scale, so the study was performed at 77 K, a temperature where the triplet excited-state lifetime is long enough.

Figure 11 exhibits the transient absorption located at 735 nm for **2** resembling that of *trans*-PhC≡CPt(PBu$_3$)$_2$C≡CPh. The former species exhibits a triplet lifetime of 48 ± 5 μs, a lifetime that compares favorably to that of the phosphorescence below 49.9 ± 0.3 μs, confirming the triplet nature of the transient species, so it is a T_1-T_n absorption. For better comparison, the transient spectrum of *trans*-PhC≡CPt(PBu$_3$)$_2$C≡CPh were recorded, and the transient band was seen at about 725 nm, similar to that of compound **2**.

Both **1** and **2** are phosphorescent in 2MeTHF at 77 K (Figure 12). The emission bands show the typical vibronic progression known for this class of compounds.[4k] The assignment for the phosphorescence for **1** and **2** is MLCT on the basis of the MO description of Figure 7 and the TDDFT described above. The photophysical data are summarized in Table 5. Compounds **1** and **2** exhibit τ_P's of ~85 and 50 μs, respectively, longer than that for the *trans*-PhC≡CPt(PBu$_3$)$_2$C≡CPh (35.0 ± 1.3 μs in 2MeTHF at 77 K; this work). This trend follows the number of methyl groups located at the *ortho*-positions (τ_P varies as 2 > 1 > 0) and may reflect the relative ease for the aryl groups to rotate about the Pt−C≡C−Ar axis. This motion may contribute to the nonradiative relaxation to the ground state. A weak fluorescence was also detected for **1** at ~405 nm, but its weak intensity prevented accurate measurements of τ_F and Φ_F. We also proposed a MLCT fluorescence.

2. Spacers 4 and 6. These spacers are fluorescent at 298 and 77 K in 2MeTHF and also phosphorescent at 77 K in 2MeTHF (Figure 13). These emissions are assigned on the basis of the small Stokes shift observed at 77 K and the short emission lifetimes for the short wavelength luminescence, and the large Stokes shift and longer lifetime for the long wavelength features (the data are available in Table 5). The 298 K fluorescence of spacer **6** is very broad and red-shifted (445 nm) with respect to the 77 K spectrum (365 nm), and the excitation spectra reasonably matched the absorption feature at 300 nm in both cases. We have no explanation for this difference except to suspect that a change in conformation in the excited state is at the origin of this phenomenon. The fluorescence lifetimes for **4** and **6** at 298 K were too short to be measured on our instrument (i.e., <0.1 ns).

Spacer **4** exhibits a single fluorescence and single phosphorescence band at 77 K, suggesting that either the *syn*- and *anti*-isomers emit at the same wavelength or one is more luminescent than the other. The fact that a double exponential is observed in the decay traces indicates that indeed both isomers may be detected.

The striking feature is that the observed emissions at both temperatures are blue-shifted with respect to the CT absorption (ethynylphenyl → quinone diimine) of the spacer. No emission was detected all the way down to 850 nm, the limit of our instrument using excitation going from 300 to 550 nm. This observation indicates that both the fluorescence and the phosphorescence arise from upper excited states in these conjugated

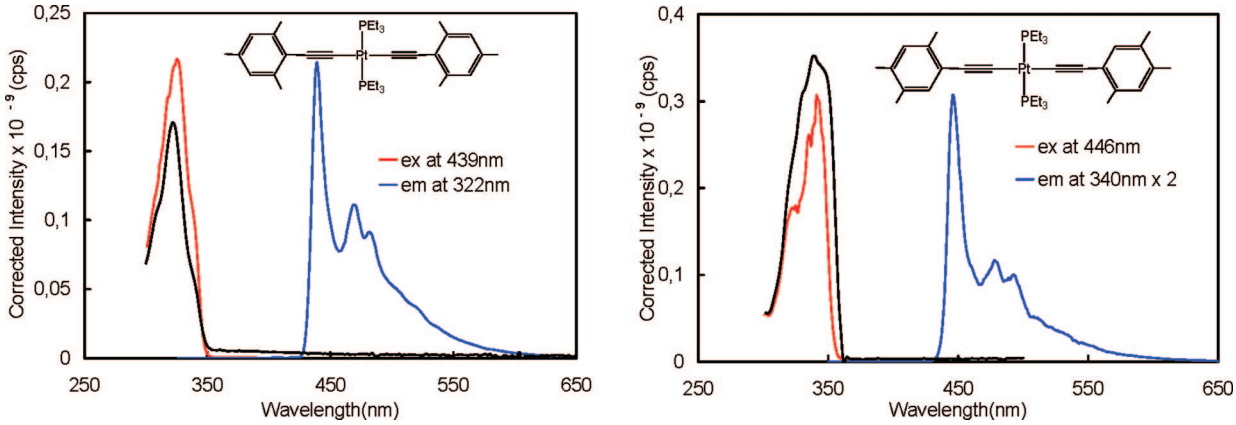

Figure 12. Phosphorescence spectra (in blue) of **1** (left) and **2** (right) in 2MeTHF at 77 K. The absorption (black) and excitation spectra (red) superimpose well.

Table 5. Photophysical Data at 77 K

compound	λ_{em} (nm) F = fluorescence, P = phosphorescence	τ_F (ns) and τ_P(μs)	Φ_P (±10%)	Φ_F (±10%)
6	365(F), 436(P), 466sh(P)	$\tau_F = 0.78 \pm 0.02$ $\tau_P = 25 \pm 2$	0.15	0.59
4	373(F), 420sh(P), 455sh(P)	$\tau_F = 0.51 \pm 0.04$ $\tau_P = 1.1 \pm 0.2$ (85%) and 11.6 ± 0.6 (15%)	[b]	[b]
1	405(F), 440(P), 470(P), 482(P)	[a] $\tau_P = 85.2 \pm 0.5$	0.38	[c]
2	446(P), 478(P), 493(P), 510sh(P)	$\tau_P = 49.9 \pm 0.3$	0.17	-
7	370(F), 444(P), 450sh(P), 475(P)487sh(P)	[a] $\tau_P = 40.1 \pm 5.6$	0.13	[c]
7′	400(F), 438(P), 450sh(P), 470(P), 480(P), 500sh(P)	$\tau_P = 125 \pm 4$	0.033	0.031
11	395(F), 465(P) 0.0033	[a] $\tau_P = 40.2 \pm 3.4$ (80%) and 92.7 ± 3.4 (20%) 0.0003		
12	420sh(F), 444sh(P), 455(P), 488(P), 503(P) 523sh(P)	$\tau_P = 80.1 \pm 3.8$	0.030	

[a] Either too weak to be measured or too short-lived for our instrument ($\tau_F < 0.1$ ns). [b] The fluorescence and phosphorescence quantum yields are not measured. Since the phosphorescence is very weak, the value was placed in the column of the fluorescence. [c] The weak fluorescence signal was strongly covered by the phosphorescence, so that it was not possible to accurately measure Φ_F.

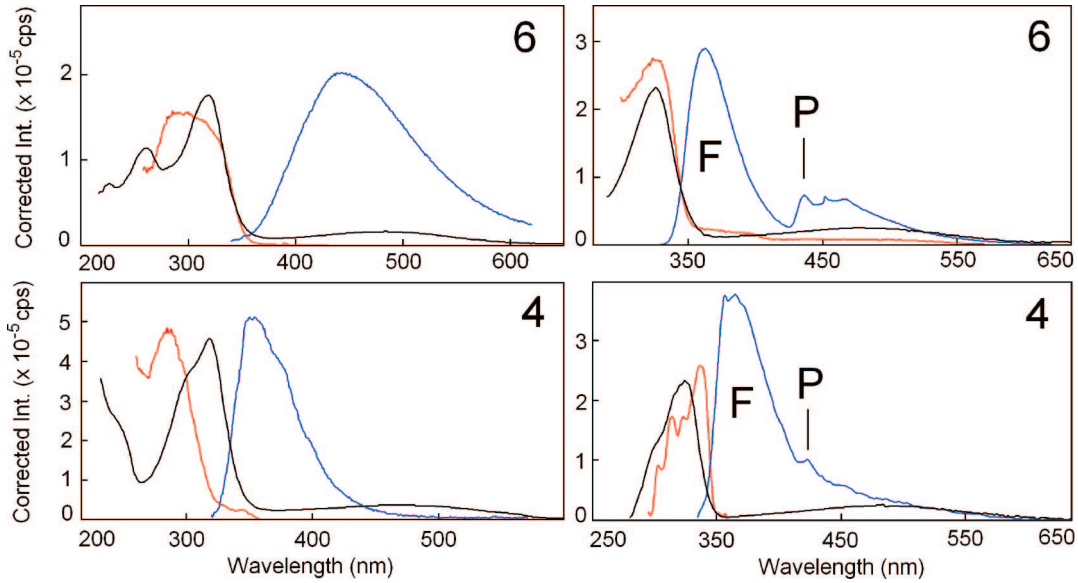

Figure 13. Phosphorescence spectra (in blue) of **6** (up) and **4** (down) in 2MeTHF at 298 K (left) and 77 K (right). The fluorescence and phosphorescence are indicated with F and P, respectively, for the 77 K spectra. On some occasions, the excitation spectra did not match perfectly the absorptions.

molecules (i.e., $S_n \rightarrow S_0$ and $T_n \rightarrow S_0$), violating Kasha's rule. Such a property is relatively rare and may be due to poor π-orbital overlaps between the ethynylbenzene and the quinone diimine fragment, as deduced from the large interplanar angle. In other words, despite conjugation the spacers act independently in the excited state, somewhat corroborating the highly localized LUMO and LUMO+n seen for **6**, **7**, and *trans*-(ligand **6**)−Pt(PEt_3)$_2$−(ligand **6**). Also, even considering that the fragments are not electronically communicating by conjugation (if this were the case) such as dyads, the lack of emission quenching by either singlet or triplet electron or energy transfers is also unusual.

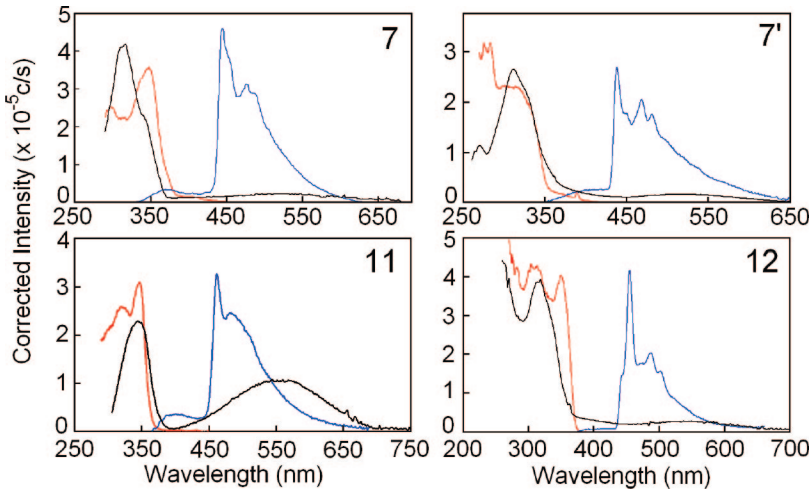

Figure 14. Phosphorescence spectra (in blue) of **7**, **7′**, **11**, and **12** in 2MeTHF at 77K. The absorption (black) and excitation spectra (red) superimpose somewhat.

Attempts were made to measure the triplet–triplet absorption spectra, notably associated with the CT states (as the τ_P values were large enough at 77 K), but were unsuccessful. The presence of N_2 bubbles in the Dewar assembly were due to the presence of high-energy laser-induced large light scatterings. No signal could be detected.

3. Model Compound 7 and Oligomers and Polymers 7′ and 10−12. These materials are not luminescent at 298 K in the solid state or in solution. However at 77 K using 2MeTHF as the solvent, two emissions attributable to fluorescence and phosphorescence (MLCT) similar to that of compounds **1** and **2** and platinum-acetylide oligomers of the type Ph(−C≡C−Pt(PEt$_3$)$_2$−C≡C−C$_4$H$_4$−)$_n$H[23] were observed for **7**, **7′**, **11**, and **12** (Figure 14), whereas no emission was observed for polymer **10**.[26] The τ_F values turned out to be shorter than the limit of our instrument (<0.1 ns). The spectra were measured at low concentrations, where no change in the spectral and photophysical properties occurred.

Several striking features are noticed. First, the magnitude of Φ_P follows that of M_n reported in Table 1 (Φ_P; **7′** (0.033) > **12** (0.030) > **11** (0.0033) > **10** (Φ_P < 0.0001)). This trend is consistent with an increase in nonradiative deactivation rates as the molecular size increases via the well-known "loose bolt" effect (higher density of vibrational levels through which nonradiative relaxation can take place).[27] On the other hand, the measured τ_P's for **7′**, **11**, and **12** (ranging from 40 to 125 μs) are of the same order of magnitude as the mononuclear model compounds **1**, **2**, and **7** (40–85 μs). This phenomenon is explained by the fact that the decay traces are dominated by the most intense emission arising from the longest lived species, which is of very low molecular weight. This polydispersity is responsible for these observed photophysical properties.

The most notable feature is the lack of low-energy emission below the CT (500–650 nm) for the oligomers and polymers. On the basis of the study of spacers **4** and **6**, this behavior is related to the properties of the spacers. Despite conjugation detected by UV–vis spectroscopy and corroborated by DFT calculations, the lack of communication in the excited state as suggested by the LUMO (Figure 9) makes the *trans*-PhC≡CPt(PEt$_3$)$_2$C≡CPh fragment and quinone diimine residue act as two weakly interacting chromophores in the excited states. Thus, this behavior provides the possibility of upper excited-state fluorescence and phosphorescence ($S_n \rightarrow S_0$ and $T_n \rightarrow S_0$) arising from the *trans*-PhC≡CPt(PEt$_3$)$_2$C≡CPh unit. This property is common to all investigated materials (**7**, **7′**, **11**, and **12**). The only exception is polymer **10**, for which no reliable emission is detected. To our knowledge, such a phenomenon is unprecedented in conjugated polymers.

Moreover, one can also preclude the presence of efficient triplet–triplet energy transfer (from the *cis*- or *trans*-PhC≡CPt(PEt$_3$)$_2$C≡CPh unit to the quinone diimine fragment), as the τ_P's for the donor (here the *cis*- or *trans*-PhC≡CPt(PEt$_3$)$_2$C≡CPh chromophore assigned on the basis of the absorption and phosphorescence maxima) remain little affected in the polymers. This observation is consistent with the conclusion that these units do not communicate efficiently in the excited states.

During the course of this investigation, delayed fluorescence was observed readily, detected from time-resolved spectroscopy in the μs time scale (SI), where both the phosphorescence and fluorescence decay at the same rate with delay times (i.e., the fluorescence/phosphorescence intensity ratio is constant). An investigation of the steady-state emission spectra vs concentration (SI) showed that the fluorescence/ phosphorescence intensity ratio was indeed a function of the latter, first suggesting the presence of aggregations at 77 K, but also allowing one to assign the mechanism of delayed fluorescence to $T_1 + T_1 \rightarrow S_1 + S_0$. The presence of aggregation also explains why no linear correlation between the intensity of the delayed fluorescence and the square of the concentration was observed.

Conclusion

A novel class of organometallic conjugated polymers were prepared and characterized in detail. These new materials are built upon two chromophores, the *cis*- and *trans*-PhC≡CPt(PEt$_3$)$_2$C≡CPh unit and the quinone diimine, often used as a building block for models of polyaniline. The key feature in this work is that the structural parameter A2 (Chart 4), directed by intramolecular steric interactions, controls or explains the variation of the M_n (and M_w) and the CT absorptivities in the title polymers. Incidentally, the position of the CT band is also a function of M_n and, thus, is indirectly a function of the angle A2. Despite the

(26) A weak emission was observed for **10**, but this emission spectrum did not resemble that for the others shown in Figure 14, and the excitation spectrum did not match the absorption one, despite the change of emission and excitation wavelength. This emission is most likely due to impurities.

(27) Turro, N. J. *Modern Molecular Photochemistry*; Benjamin/Cummings: Menlo Park, 1978.

obvious conjugation in the ground state, the two chromophores do not communicate efficiently in the excited states. This property provides the possibility of observing localized excited states. For this reason, upper excited-state emission arising from the *cis*- or *trans*-PhC≡CPt(PEt_3)$_2$C≡CPh units is detected. This interesting phenomenon may well be associated with the large interplanar angles between the −C≡CPh residue and the quinone diimine An unpublished geometry optimization by DFT calculations performed on the protonated (+ 4 H^+) model compound *trans*-(ligand **6**)−Pt(PEt_3)$_2$−(ligand **6**) (where the H^+ are placed on the N atoms) shows that the structure of the resulting compound is totally planar and delocalized. In addition, the protonated versions of ligands **2**, **3**, **4**, and **5** in the presence of acids exhibit reversible oxidation waves. On the basis of these observations, the reported polymers in this work may be potential candidates for the design of novel conducting polymers resembling that of an organometallic version of polyaniline. Future works in this area are in progress.

Acknowledgment. This work was supported by the Natural Science and Engineering Research Council of Canada (NSERC). The authors thank Dr. Frédéric Brisach, Mr. Smail Dahmane, and Dr. Regina Zamojska for the measurements of several preliminary UV–vis spectra, of the DSC traces, and of TGA traces, respectively.

Supporting Information Available: Synthesis of **4′**, cyclic voltammograms for the model compounds PhC≡CPt(PEt_3)$_2$C≡CPh, **1**−**3**, **5**, **6**, and **10**−**12**, TGA traces for the polymers **7′** and **10**−**12**, DSC trace for polymer **10** in the 80–180 °C window, picture of stand-alone polymer **10**, frontier MOs for the cyclic compound **7**, time-resolved spectra of **1**, **2**, **7**, **7′**, **11**, and **12**, crystal data and structure refinements for **1**−**9** and **4′**, and experimental section. This material is available free of charge via the Internet at http://pubs.acs.org.

OM7010563